Earthquakes and Structures, *Vol. 10, No. 5 (2016) 989-1012*
DOI: http://dx.doi.org/10.12989/eas.2016.10.5.989

Structural response analysis in time and frequency domain considering both ductility and strain rate effects under uniform and multiple-support earthquake excitations

Guohuan Liu[1,2], Jijian Lian[1,2], Chao Liang[*1,2] and Mi Zhao[3]

[1]*State Key Laboratory of Hydraulic Engineering Simulation and Safety, Tianjin University, 300072, Tianjin, China*
[2]*School of Civil Engineering, Tianjin University, 300072, Tianjin, China*
[3]*College of Architecture and Civil Engineering, Beijing University of Technology, 100124, Beijing, China*

(Received November 1, 2015, Revised December 8, 2015, Accepted February 23, 2016)

Abstract. The structural dynamic behavior and yield strength considering both ductility and strain rate effects are analyzed in this article. For the single-degree-of-freedom (SDOF) system, the relationship between the relative velocity and the strain rate response is deduced and the strain rate spectrum is presented. The ductility factor can be incorporated into the strain rate spectrum conveniently based on the constant-ductility velocity response spectrum. With the application of strain rate spectrum, it is convenient to consider the ductility and strain rate effects in engineering practice. The modal combination method, i.e., square root of the sum of the squares (SRSS) method, is employed to calculate the maximum strain rate of the elastoplastic multiple-degree-of-freedom (MDOF) system under uniform excitation. Considering the spatially varying ground motions, a new response spectrum method is developed by incorporating the ductility factor and strain rate into the conventional response spectrum method. In order to further analyze the effects of strain rate and ductility on structural dynamic behavior and yield strength, the cantilever beam (one-dimensional) and the triangular element (two-dimensional) are taken as numerical examples to calculate their seismic responses in time domain. Numerical results show that the permanent displacements with and without considering the strain rate effect are significantly different from each other. It is not only necessary in theory but also significant in engineering practice to take the ductility and strain rate effects into consideration.

Keywords: strain rate effect; ductility effect; multiple-support earthquake excitations; strain rate spectrum; response spectrum method

1. Introduction

The yield strength and dynamic behaviors of most materials involved in civil engineering are sensitive to strain rate. Currently, much attention is focused on the strain rate sensitivities for many kinds of materials. Huh *et al.* (2009) presented stress-strain curves of steel sheets for an auto-body obtained at intermediate strain rates with a servo-hydraulic type high speed tensile testing

*Corresponding author, E-mail: liangchao_0016@sina.cn

http://www.techno-press.com/journals/eas&subpage=7 ISSN: 2092-7614 (Print), 2092-7622 (Online)

machine. Li and Li (2010) investigated the dynamic properties of reinforcing steels of various strengths using a MTS New 810 electro-hydraulic servo-controlled testing system with a range of strain rate between 2.5×10^{-4}/s and 0.1/s, which covers the range that might be experienced during earthquakes, and developed a rate-dependent cyclic constitutive model of reinforcing steel through improving the Hoehler model. Furthermore, Li and Li (2012) studied the effects of strain rate on the reinforced concrete structure under seismic loading. Based on the test results, dynamic increasing factors (DIF) which are functions of strain rate and quasi-static yielding strength of reinforcing steel are gotten. These results provide a reference for reinforced concrete frame structure in seismic design. The effects of strain rate on strength and deformation characteristics of soil-lime were investigated by Alzubaidi and Lafta (2013). It is observed that for soil-lime mixture at different curing periods, the undrained shear strength, initial modulus of elasticity and the cohesion increase to a maximum and then decrease with increasing strain rate.

In earthquake engineering, the effect of strain rate on the structural dynamic behavior is ignored in the early years. With the application of modern computing facilities and methods, more and more researchers pay attention to the strain rate effect in engineering practice. Shing and Mahin (1988) conducted a series of pseudo-dynamic tests considering the strain rate effects of structures concluded that the dynamic strength is approximately 30% higher than the static strength. A dynamic constitutive model for the concrete structure in seismic design practice is recommended by CEBFIP model code (1990). Cervera *et al.* (1996) analyzed the Koyna dam considering the strain rate effect of concrete. The results show that the strain rate $\dot{\varepsilon}$ is higher than $10^{-3}\mathrm{s}^{-1}$ and the dynamic tensile strength increases by 45%. Chopra (2001, 2004) studied the relationship between the peak deformations of inelastic and corresponding elastic SDOF systems and obtained the fitting formulae for the relationship. Wang *et al.* (2013) investigated the effects of ultimate strain and strain rate of materials on the collapse mechanism, routine and capacity of transmission tower-line system. Results show that the strain rate has a significant influence on the top displacement and base shear of tower under certain seismic records. Li and Larry (2013) presented research that used single-degree-of-freedom systems to represent low-ductility CBFs, where brace fracture causes a sudden loss of strength and stiffness. For the cases considered, the ductility capacity of the reserve system was typically a more critical constraint than global drift capacity, and reserve capacity is demonstrated to appreciably influence seismic collapse behavior, whereas primary system strength has a small influence.

The response spectrum regarded as a basic concept in earthquake engineering provides a convenient means to summarize the peak response of all possible elastic SDOF systems subjected to a particular component of ground motion (Hao 1991, Kiureghian and Neumnhofer 1992, Hao and Xiao 1996, Su *et al.* 2006, Yu and Zhou 2008, Xu 2010, Guo 2013, Su and Shi 2013, Tian *et al.* 2010, 2014, Carlson *et al.* 2014). Therefore, the strain rate spectrum is presented in this paper and a new response spectrum method based on structural ductility and strain rate spectrum is developed for the dynamic analysis of the MDOF multi-support system.

2. Review of the earthquake response for the elastoplastic system

The well-known governing equation of the elastic SDOF system is

$$m\ddot{u} + c\dot{u} + ku = -m\ddot{u}_g(t) \tag{1}$$

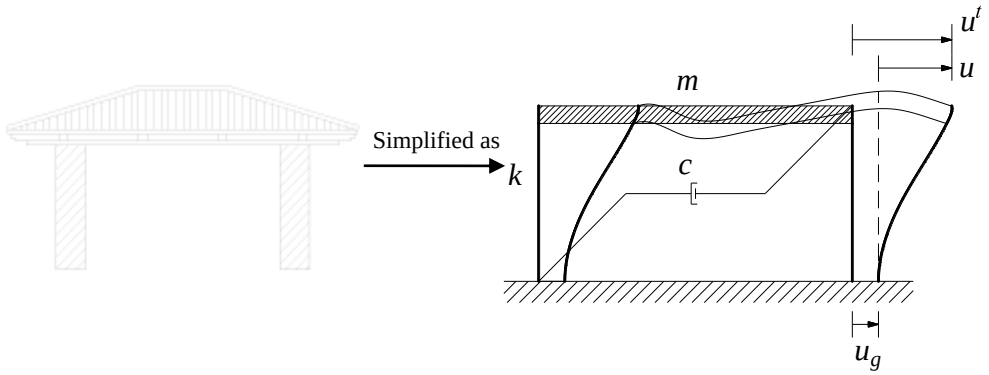

(a) The actual structure (b) The ideal SDOF system

*u^t and u_g denote the total displacement and the prescribed support displacement, respectively

Fig. 1 The actual structure and corresponding ideal SDOF system

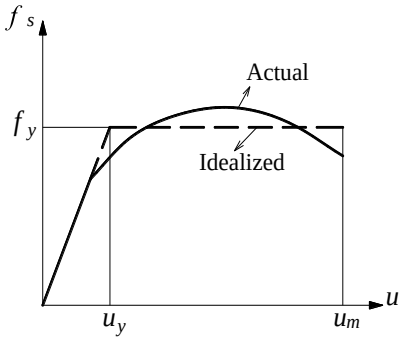

Fig. 2 Force-deformation curves during initial loading

where, m, c and k are the mass, damping and stiffness of the SDOF system, respectively; $\ddot{u}$, $\dot{u}$ and u are the acceleration, velocity and deformation response of the SDOF system, respectively; $\ddot{u}_g(t)$ is the prescribed support acceleration. As shown in Fig. 1, the deformation of the SDOF system is given.

For the elastoplastic system, the force-deformation relation is no longer single-valued if the system is unloading or reloading, and the resisting force f_s expressed as ku in Eq. (1) depends on the prior history of the system deformation and whether the deformation is currently increasing ($\dot{u} > 0$) or decreasing ($\dot{u} < 0$). Therefore, the governing equation for elastoplastic SDOF system can be expressed as

$$m\ddot{u} + c\dot{u} + f_s(u, \dot{u}) = -m\ddot{u}_g(t) \tag{2}$$

The force-deformation relation for a structure during its initial loading is given in Fig. 2, and the parameters u_y and f_y represent the yield deformation and strength. It is convenient to idealize the actual curve by a perfect elastoplastic force-deformation relation. The elastoplastic approximation to the actual force-deformation curve is shown in Fig. 2, and the areas under the two curves are the same at the selected value of the maximum displacement u_m. As illustrated in Fig. 3, the yield forces are the same in the two directions of deformation. Unloading from a point

of the maximumtable deformation takes place along a path parallel to the initial elastic branch. Similarly, reloading from a point of the minimum deformation takes place along a path parallel to the initial elastic branch. The maximum and minimum values of the resisting force (i.e., yield strength) for deformations in excess of the yield deformation are f_y.

It is desirable to evaluate the peak deformation of an elastoplastic system due to prescribed earthquake ground motion and to compare this deformation to the peak deformation caused by the same excitation in the corresponding elastic system. As illustrated in Fig. 4, this elastic system is assumpted to have the same stiffness as the stiffness of the elastoplastic system during its initial loading. Both mass and damping are the same for the two systems. Therefore, the natural vibration period of the corresponding elastic system is the same as the period of the elastoplastic system undergoing small ($u \leq u_y$) oscillations.

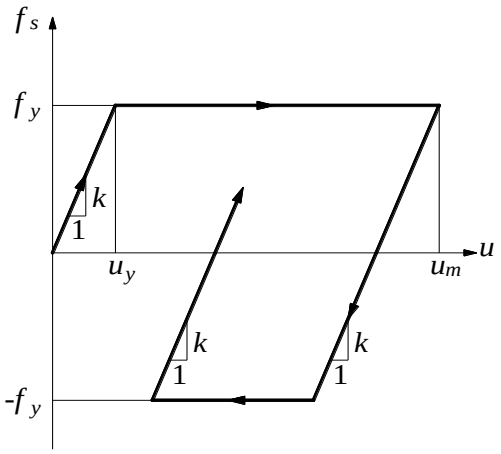

Fig. 3 Hysteretic curve for ideal elastoplastic system

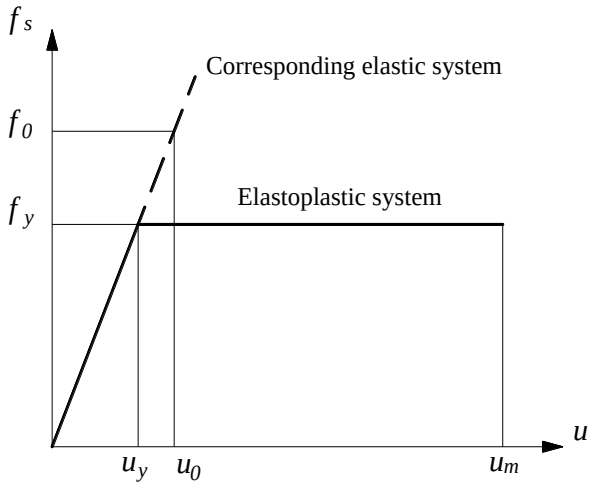

*f_0 and u_0 are the peak values of the earthquake-induced resisting force and deformation in the corresponding elastic system

Fig. 4 Force-deformation relations of the elastoplastic and elastic systems

The normalized yield strength $\bar{f_y}$ of an elastoplastic system is defined as

$$\bar{f_y} = \frac{f_y}{f_0} = \frac{u_y}{u_0} \tag{3}$$

It is noted that f_0 can also be regarded as the minimum strength required for the structure to remain within its linearly elastic limit during the ground motion. If the normalized yield strength $\bar{f_y} < 1$, the deformation of system will exceed its linearly elastic limit; and if $\bar{f_y} \geq 1$, plastic deformation won't occur under seismic excitation.

The peak deformation of the elastoplastic system due to the prescribed ground motion is denoted by u_m. It is meaningful to normalize u_m relative to the yield deformation of the system

$$\mu = \frac{u_m}{u_y} \tag{4}$$

where the dimensionless rate μ is called the ductility factor.

According to Eq. (2), the following equation can be obtained

$$\ddot{u} + 2\xi\omega_n\dot{u} + \omega_n^2 u_y \tilde{f_s}(u, \dot{u}) = -\ddot{u}_g(t) \tag{5}$$

where

$$\omega_n = \sqrt{\frac{k}{m}} \tag{6}$$

$$\xi = \frac{c}{2m\omega_n} \tag{7}$$

$$f_y = ku_y \tag{8}$$

$$\tilde{f_s}(u, \dot{u}) = \frac{f_s(u,\dot{u})}{f_y} \tag{9}$$

in which the quantity ω_n is the natural frequency of the elastoplastic system vibrating within its linearly elastic range (i.e., $u \leq u_y$). Obviously, ω_n is also the natural frequency of the corresponding elastic system. Similarly, ξ is the damping rate of the system based on the critical damping $2m\omega_n$ of the elastoplastic system vibrating within its linearly elastic range, and ξ also represents the damping ratio of the corresponding elastic system. Moreover, the function $\tilde{f_s}(u, \dot{u})$ describes the force-deformation relation in a partially dimensionless form.

The relationship between the ductility factor μ and the deformation response $u(t)$ can be expressed as follows

$$u(t) = u_y\mu(t) \tag{10}$$

$$\dot{u}(t) = u_y\dot{\mu}(t) \tag{11}$$

$$\ddot{u}(t) = u_y\ddot{\mu}(t) \tag{12}$$

Substituting Eqs. (10)-(12) into Eq. (5) yields

$$\ddot{\mu} + 2\xi\omega_n\dot{\mu} + \omega_n^2\tilde{f_s}(\mu, \dot{\mu}) = -\omega_n^2\frac{\ddot{u}_g(t)}{a_y} \tag{13}$$

where

$$a_y = \frac{f_y}{m} \tag{14}$$

$$\tilde{f}_s(\mu, \dot{\mu}) = \frac{f_s(\mu, \dot{\mu})}{f_y} \tag{15}$$

in which the quantity a_y can be interpreted as the acceleration of the mass necessary to produce the yield force f_y, and $\tilde{f}_s(\mu, \dot{\mu})$ is the force-deformation relation in normalized form.

3. Deduction of the strain rate spectrum for the elastoplastic system

It is clear that for a given $\ddot{u}_g(t)$, the deformation response $u(t)$ of the system depends only on the natural frequency ω_n or natural period $T_n = 2\pi/\omega_n$, damping ratio ξ and the yield deformation u_y. Thus, the deformation calculated by Eq. (5) can be written as

$$u \equiv u\left(t, T_n, \xi, u_y\right) \tag{16}$$

Furthermore, the velocity and acceleration response calculated by Eq. (5) can be expressed as follows

$$\dot{u} \equiv \dot{u}\left(t, T_n, \xi, u_y\right) \tag{17}$$

$$\ddot{u} \equiv \ddot{u}\left(t, T_n, \xi, u_y\right) \tag{18}$$

Considering the maximum values of the displacement, velocity and acceleration responses within the time domain, the following response spectrums are obtained

$$u_s\left(T_n, \xi, u_y\right) = \max_t \left|u\left(t, T_n, \xi, u_y\right)\right| \tag{19}$$

$$\dot{u}_s\left(T_n, \xi, u_y\right) = \max_t \left|\dot{u}\left(t, T_n, \xi, u_y\right)\right| \tag{20}$$

$$\ddot{u}_s\left(T_n, \xi, u_y\right) = \max_t \left|\ddot{u}\left(t, T_n, \xi, u_y\right)\right| \tag{21}$$

where u_s, $\dot{u}_s$ and $\ddot{u}_s$ denote the deformation, relative velocity and acceleration response spectrum, respectively.

The deformation of an arbitrary point within the system can be calculated by the product of the nodal deformation and the shape function as shown in the following equation

$$z(x, t) = \psi(x) u\left(t, T_n, \xi, u_y\right) \tag{22}$$

where $z(x, t)$ denotes the deformation of a certain point; $\psi(x)$ represents the shape function of the system. Note that the strain is the spatial derivative of the deformation function, the following equations can be obtained

$$\varepsilon = E(z) = E(\psi) u\left(t, T_n, \xi, u_y\right) \tag{23}$$

$$E = \frac{\partial}{\partial x} \tag{24}$$

where ε and E denote the normal strain and strain operator in the x direction, respectively. It is noted that the present paper is mainly focus on displacement-based element formulations. Further researches are needed if the force-based element formulations are adopted.

The time derivative of Eq. (23) is expressed as

$$\dot{\varepsilon} = E(\psi)\dot{u}\left(t, T_n, \xi, u_y\right) \tag{25}$$

where $\dot{u}$ and $\dot{\varepsilon}$ are the relative velocity and the strain rate response, respectively.

Considering the maximum value of ε and $\dot{\varepsilon}$ within the time domain, the following formulae are obtained

$$|\varepsilon|_{max} = |E(\psi)|\left|u\left(t, T_n, \xi, u_y\right)\right|_{max} = |E(\psi)|u_s\left(T_n, \xi, u_y\right) \tag{26}$$

$$|\dot{\varepsilon}|_{max} = |E(\psi)|\left|\dot{u}\left(t, T_n, \xi, u_y\right)\right|_{max} = |E(\psi)|\dot{u}_s\left(T_n, \xi, u_y\right) \tag{27}$$

According to Eq. (27), the relationship between the maximum strain rate $|\dot{\varepsilon}|_{max}$ and the velocity response spectrum $\dot{u}_s\left(T_n, \xi, u_y\right)$ can be calculated by

$$\dot{u}_s\left(T_n, \xi, u_y\right) = \frac{|\dot{\varepsilon}|_{max}}{|E(\psi)|} \tag{28}$$

Due to the lack of velocity response spectrum for elastoplastic system, the pseudo-velocity response spectrum can be used instead. Over the medium-period range (i.e., $0.1\ \text{s} < T_n < 5\ s$) the value of pseudo-velocity is very close to the value of velocity. Furthermore, it is convenient for the following analyses that the frequently used deformation and pseudo-velocity response spectrums for both elastic and elastoplastic systems are directly given by Chopra (2001). In addition, the relationship between deformation, pseudo-velocity and pseudo-acceleration can be expressed as

$$u = \frac{T_n}{2\pi}\dot{u}_p = \left(\frac{T_n}{2\pi}\right)^2 \ddot{u}_p \tag{29}$$

where $\dot{u}_p$ and $\ddot{u}_p$ denote the pseudo-velocity and pseudo-acceleration, respectively.

As shown in Figs. 5(a)-(b), the elastic pseudo-acceleration and pseudo-velocity response spectrums taken from reference (Chopra 2001) are given and, in addition, the damping rate ξ is set to 5%. A simple approach to generate a constant-ductility spectrum for the elastoplastic system is given by Chopra (2001, 2004). In this approach, the constant-ductility spectrum is calculated by multiplying the elastic spectrum by the normalized yield strength $\bar{f}_y$ of the elastoplastic system. The relationship between normalized yield strength $\bar{f}_y$ and ductility factor μ is expressed as

$$\bar{f}_y = \begin{cases} 1 & T_n < T_a \\ (2\mu - 1)^{-1/2} & T_b < T_n < T_{c'} \\ \mu^{-1} & T_n > T_c \end{cases} \tag{30}$$

where the period values T_a and T_b are fixed and set to 0.03 s and 0.125 s respectively for the earthquake motions on firm ground. Although the parameters $T_{c'}$ and T_c are involved in Eq. (30), they are not essential for the calculation of constant-ductility spectrum. The detailed analysis can be seen in references (Chopra 2001, 2004). According to Eq. (3), $\bar{f}_y$ is the ratio of f_y and f_0. Herein, f_y can be interpreted as the strength demand for the structure with the given ductility

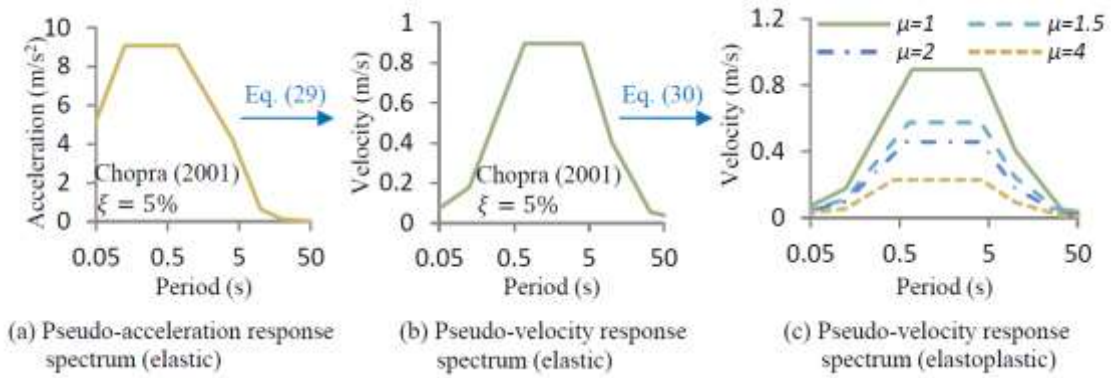

(a) Pseudo-acceleration response spectrum (elastic) (b) Pseudo-velocity response spectrum (elastic) (c) Pseudo-velocity response spectrum (elastoplastic)

*Semilog coordinates are adopted

Fig. 5 Calculation process from elastic response spectrum to elastoplastic response spectrum

factor (Chopra 2001, Zhai and Xie 2007). In engineering practice, it is desired to determine the strength demand f_y of the system to limit the ductility demand imposed by the ground motion to a specified value.

According to the above analysis, the maximum strain rate can be obtained if the natural period and damping ratio of the SDOF structure are given and the shape function is defined. Two exemplary structures are given in Fig. 6 and the shape functions are defined as

$$\psi_c = \frac{x-x_1}{x_2-x_1} \tag{31}$$

$$\psi_t = \frac{x_i y_j - x_i y_j - (y_j - y_i)x + (x_j - x_i)y}{(x_i y_j + x_j y_m + x_m y_i) - (x_i y_m + x_j y_i + x_m y_j)} \tag{32}$$

where ψ_c denotes the shape function of cantilever beam at node 2 and ψ_t denotes the shape function of triangular element at node *m*; *x* and *y* denote the coordinate values; the subscripts 1, 2, *i*, *j* and *m* denote the different nodes or supports. The deformation of support 1, node *i* and node *j* remains zero during seismic excitation, thus the shape functions of support 1, node *i* and node *j* are unnecessary to be taken into consideration.

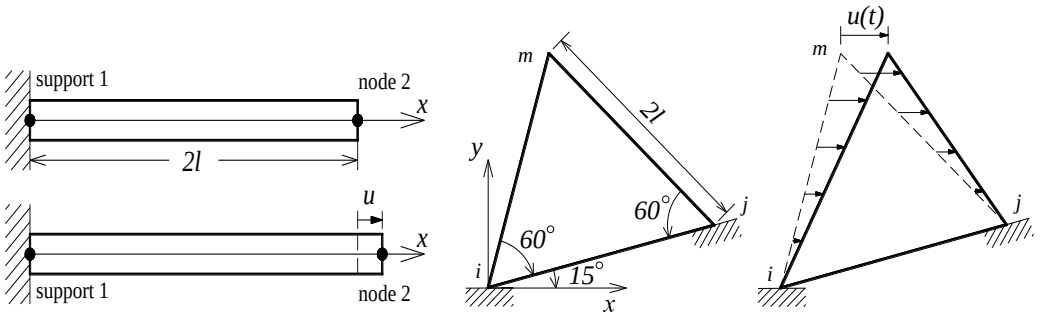

(a) Cantilever beam (one-dimensional) (b) Triangular element (two-dimensional)

*Supports *i* and *j* are completely fixed

Fig. 6 Exemplary structures

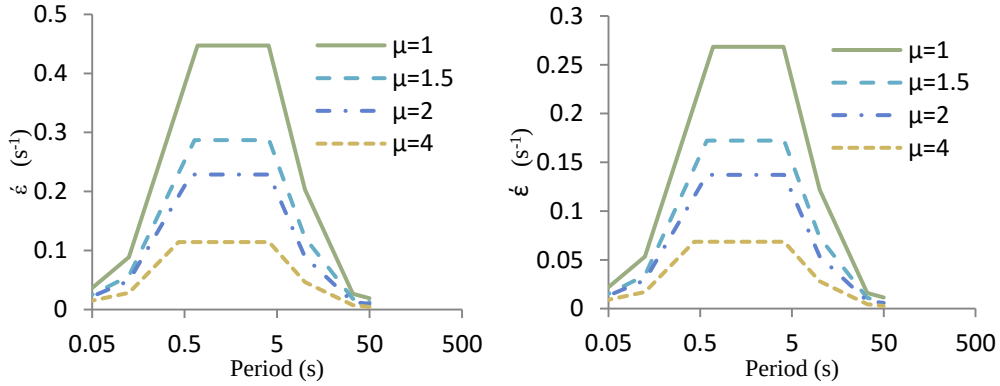

(a) Cantilever beam (b) Triangular element

Fig. 7 Strain rate spectrums considering the ductility factor

The strain operators of the cantilever beam and triangular element, i.e., $E(\psi_c)$ and $E(\psi_t)$, can be expressed as

$$|E(\psi_c)| = \frac{1}{x_2 - x_1} \tag{33}$$

$$|E(\psi_t)| = \frac{(y_j - y_i)}{(x_i y_j + x_j y_m + x_m y_i) - (x_i y_m + x_j y_i + x_m y_j)} \tag{34}$$

For the two exemplary structures, $|E(\psi_c)|$ and $|E(\psi_t)|$ are equal to 0.5 and 0.3, respectively. Then, the strain rate spectrums calculated by Eq. (28) is given in Fig. 7.

4. Deduction of multiple-support response spectrum method considering strain rate effect

The dynamic equation for a discrete, *N*-degree-of-freedom elastic system subjected to *m* support motions can be written in following matrix form (Clough and Penzien 1993)

$$\begin{bmatrix} \boldsymbol{M} & \boldsymbol{M}_c \\ \boldsymbol{M}_c^{\boldsymbol{T}} & \boldsymbol{M}_g \end{bmatrix} \begin{Bmatrix} \ddot{\boldsymbol{x}} \\ \ddot{\boldsymbol{u}}_g \end{Bmatrix} + \begin{bmatrix} \boldsymbol{C} & \boldsymbol{C}_c \\ \boldsymbol{C}_c^T & \boldsymbol{C}_g \end{bmatrix} \begin{Bmatrix} \dot{\boldsymbol{x}} \\ \dot{\boldsymbol{u}}_g \end{Bmatrix} + \begin{bmatrix} \boldsymbol{K} & \boldsymbol{K}_c \\ \boldsymbol{K}_c^T & \boldsymbol{K}_g \end{bmatrix} \begin{Bmatrix} \boldsymbol{x} \\ \boldsymbol{u}_g \end{Bmatrix} = \begin{Bmatrix} \boldsymbol{0} \\ \boldsymbol{P} \end{Bmatrix} \tag{35}$$

where, $\boldsymbol{M}$, $\boldsymbol{C}$ and $\boldsymbol{K}$ denote the $N \times N$ mass, damping and stiffness matrices associated with the unconstrained degrees of freedom, respectively; $\boldsymbol{M}_g$, $\boldsymbol{C}_g$ and $\boldsymbol{K}_g$ represent the $m \times m$ mass, damping and stiffness matrices associated with the support degrees of freedom, and *m* denotes the numbers of constrained degrees of freedom; $\boldsymbol{M}_c$, $\boldsymbol{C}_c$ and $\boldsymbol{K}_c$ represent $N \times m$ coupling mass, damping and stiffness matrices associated with both unconstrained and support degrees of freedom; $\boldsymbol{P}$ denotes the *m*-vector of reacting forces at the support degrees of freedom; $\boldsymbol{y}$ represents the total displacement vector at the unconstrained degrees of freedom; $\ddot{\boldsymbol{u}}_g$, $\dot{\boldsymbol{u}}_g$ and $\boldsymbol{u}_g$ denote the *m*-vector of prescribed support acceleration, velocity and displacement, respectively.

Expanding Eq. (35) gives

$$\boldsymbol{M}\ddot{\boldsymbol{x}} + \boldsymbol{M}_c\ddot{\boldsymbol{u}}_g + \boldsymbol{C}\dot{\boldsymbol{x}} + \boldsymbol{C}_c\dot{\boldsymbol{u}}_g + \boldsymbol{K}\boldsymbol{x} + \boldsymbol{K}_c\boldsymbol{u}_g = \boldsymbol{0} \tag{36}$$

It is common to decompose the response $\boldsymbol{x}$ into pseudo-static component $\boldsymbol{x}^s$ and dynamic component $\boldsymbol{x}^d$ as following equation

$$\boldsymbol{x} = \boldsymbol{x}^s + \boldsymbol{x}^d \tag{37}$$

Substituting Eq. (37) into Eq. (36) gives

$$\boldsymbol{M}\ddot{\boldsymbol{x}}^d + \boldsymbol{C}\dot{\boldsymbol{x}}^d + \boldsymbol{K}\boldsymbol{x}^d = -\left[\left(\boldsymbol{M}\ddot{\boldsymbol{x}}^s + \boldsymbol{M}_c\ddot{\boldsymbol{u}}_g\right) + \left(\boldsymbol{C}\dot{\boldsymbol{x}}^s + \boldsymbol{C}_c\dot{\boldsymbol{u}}_g\right) + \left(\boldsymbol{K}\boldsymbol{x}^s + \boldsymbol{K}_c\boldsymbol{u}_g\right)\right] \tag{38}$$

It is well known that the term $\left(\boldsymbol{K}\boldsymbol{x}^s + \boldsymbol{K}_c\boldsymbol{u}_g\right)$ in the right-hand side of Eq. (38) remains zero. Therefore, the following relationship can be obtained

$$\boldsymbol{x}^s = -\boldsymbol{K}^{-1}\boldsymbol{K}_c\boldsymbol{u}_g = \boldsymbol{R}\boldsymbol{u}_g \tag{39}$$

where $\boldsymbol{R}$ denotes the influence matrix.

Substituting Eq. (39) into Eq. (38) yields

$$\boldsymbol{M}\ddot{\boldsymbol{x}}^d + \boldsymbol{C}\dot{\boldsymbol{x}}^d + \boldsymbol{K}\boldsymbol{x}^d = -(\boldsymbol{M}\boldsymbol{R} + \boldsymbol{M}_c)\ddot{\boldsymbol{u}} - (\boldsymbol{C}\boldsymbol{R} + \boldsymbol{C}_c)\dot{\boldsymbol{u}} \approx -(\boldsymbol{M}\boldsymbol{R} + \boldsymbol{M}_c)\ddot{\boldsymbol{u}} \tag{40}$$

where the right-hand side is approximated by neglecting the damping forces, which are usually much smaller than the inertia forces on the same side. It is noted that $\boldsymbol{M}_c = 0$ if a lumped-mass model is used.

The circular frequency $\boldsymbol{\omega}$ and mode shape $\boldsymbol{\Phi}$ can be calculated by the following equation.

$$[\boldsymbol{K} - \boldsymbol{\omega}^2\boldsymbol{M}]\boldsymbol{\Phi} = \boldsymbol{0} \tag{41}$$

The vectors of vibration mode and generalized coordinate are given in Eqs. (42)-(43)

$$\boldsymbol{\Phi} = [\boldsymbol{\phi}_1 \cdots \boldsymbol{\phi}_n] \tag{42}$$

$$\boldsymbol{y} = [y_1 \cdots y_n] \tag{43}$$

Substitute transformation

$$\boldsymbol{x}^d = \boldsymbol{\Phi}\boldsymbol{y} \tag{44}$$

into Eq. (40), the decoupled dynamic equations for the MDOF system under uniform and multiple-support excitations are expressed respectively as follows

$$\ddot{y}_i + 2\xi_i\omega_i\dot{y}_i + \omega_i^2 y_i = -\frac{(\boldsymbol{\Phi}_i)^T\boldsymbol{M}\boldsymbol{R}}{(\boldsymbol{\Phi}_i)^T\boldsymbol{M}\boldsymbol{\Phi}_i}\ddot{u}_g(t),\ i = 1, \cdots, n \tag{45}$$

$$\ddot{y}_i + 2\xi_i\omega_i\dot{y}_i + \omega_i^2 y_i = -\sum_{k=1}^{m}\beta_{ki}\ddot{u}_k(t),\ i = 1, \cdots, n \tag{46}$$

where the subscript *i* denotes the mode number, and the index *k* denotes the degrees of freedom associated with the prescribed support motions; β_{ki} represents the modal participation factor given by

$$\beta_{ki} = \frac{(\boldsymbol{\Phi}_i)^T(\boldsymbol{M}\boldsymbol{r}_k + \boldsymbol{M}_c\boldsymbol{i}_k)}{(\boldsymbol{\Phi}_i)^T\boldsymbol{M}\boldsymbol{\Phi}_i} \tag{47}$$

in which $\boldsymbol{r}_k$ is the k^{th} column of $\boldsymbol{R}$ and $\boldsymbol{i}_k$ is the k^{th} column of an $m \times m$ identity matrix.

For the MDOF system under uniform excitation, the strain rate responses of corresponding

SDOF systems can be calculated using Eqs. (28) and (45). Then, the total strain rate and dynamic response of the MDOF structure can be obtained by the modal combination method (Clough 1962, Singh and Mehta 1983, Sinha and Igusa 1995).

For the MDOF system under multiple-support excitations, it is convenient to define a normalized modal response $s_{ki}(t)$, representing the response of a single-degree-of-freedom oscillator of unit mass, frequency ω_i and damping ξ_i, which is subjected to the base motion $\ddot{u}_k(t)$. Thus, $s_{ki}(t)$ satisfies

$$\ddot{s}_{ki} + 2\xi_i\omega_i\dot{s}_{ki} + \omega_i^2 s_{ki} = -\ddot{u}_k(t) \tag{48}$$

The relationship between $y_i(\mathrm{t})$ and $s_{ki}(t)$ is given as

$$y_i(\mathrm{t}) = \sum_{k=1}^{m} \beta_{ki} s_{ki}(t) \tag{49}$$

Combining Eqs. (25) and (37), the strain rate response can be expressed as

$$\dot{\boldsymbol{\varepsilon}} = E(\psi)[\dot{x}^s(t) + \dot{x}^d(t)] \tag{50}$$

Substituting Eqs. (39) and (44) into Eq. (50) yields

$$\dot{\boldsymbol{\varepsilon}}'(t) = \sum_{k=1}^{m} \boldsymbol{a}_k \dot{u}_k(t) + \sum_{k=1}^{m}\sum_{i=1}^{N} \boldsymbol{b}_{ki}\dot{s}_{ki}(t) \tag{51}$$

where $\dot{\boldsymbol{\varepsilon}}'(t)$ denotes the strain rate response under multiple-support excitations; $\boldsymbol{a}_k$ and $\boldsymbol{b}_{ki}$ denote the effective influence factors and effective modal participation factors, defined as

$$\boldsymbol{a}_k = E(\psi)\boldsymbol{r}_k \tag{52}$$

$$\boldsymbol{b}_{ki} = E(\psi)\boldsymbol{\phi}_i\beta_{ki} \tag{53}$$

From Eq. (51), the PSD of the strain rate response can be written in the following form

$$\begin{aligned} G'_{\dot{\boldsymbol{\varepsilon}}\dot{\boldsymbol{\varepsilon}}}(i\omega) = {} & \sum_{k=1}^{m}\sum_{l=1}^{m} \boldsymbol{a}_k\boldsymbol{a}_l G_{\dot{u}_k\dot{u}_l}(i\omega) + 2\sum_{k=1}^{m}\sum_{l=1}^{m}\sum_{j=1}^{N} i\omega\boldsymbol{a}_k\boldsymbol{b}_{lj}H_j(-i\omega)\, G_{\dot{u}_k\ddot{u}_l}(i\omega) + \\ & \sum_{k=1}^{m}\sum_{l=1}^{m}\sum_{i=1}^{N}\sum_{j=1}^{N} (-\omega^2)\boldsymbol{b}_{ki}\boldsymbol{b}_{lj}H_i(i\omega)H_j(-i\omega)G_{\ddot{u}_k\ddot{u}_l}(i\omega) \end{aligned} \tag{54}$$

in which $G'_{xy}(i\omega)$ denotes the cross-PSD of processes *x* and *y*.

Integrating Eq. (54) over the frequency domain $-\infty < \omega < \infty$, the mean-square response is

$$\begin{aligned} (\sigma'_{\dot{\boldsymbol{\varepsilon}}})^2 = {} & \sum_{k=1}^{m}\sum_{l=1}^{m} \boldsymbol{a}_k\boldsymbol{a}_l\rho_{\dot{u}_k\dot{u}_l}\sigma_{\dot{u}_k}\sigma_{\dot{u}_l} + 2\sum_{k=1}^{m}\sum_{l=1}^{m}\sum_{j=1}^{N} \boldsymbol{a}_k\boldsymbol{b}_{lj}\rho_{\dot{u}_k\dot{s}_{lj}}\sigma_{\dot{u}_k}\sigma_{\dot{s}_{lj}} + \\ & \sum_{k=1}^{m}\sum_{l=1}^{m}\sum_{i=1}^{N}\sum_{j=1}^{N} \boldsymbol{b}_{ki}\boldsymbol{b}_{lj}\rho_{\dot{s}_{ki}\dot{s}_{lj}}\sigma_{\dot{s}_{ki}}\sigma_{\dot{s}_{lj}} \end{aligned} \tag{55}$$

in which, $\rho_{\dot{u}_k\dot{u}_l}$, $\rho_{\dot{u}_k\dot{s}_{lj}}$ and $\rho_{\dot{s}_{ki}\dot{s}_{lj}}$ are cross-correlation coefficients defined by

$$\rho_{\dot{u}_k\dot{u}_l} = \frac{1}{\sigma_{\dot{u}_k}\sigma_{\dot{u}_l}}\int_{-\infty}^{\infty} G_{\dot{u}_k\dot{u}_l}(i\omega)\, d\omega \tag{56}$$

$$\rho_{\dot{u}_k\dot{s}_{lj}} = \frac{1}{\sigma_{\dot{u}_k}\sigma_{\dot{s}_{lj}}}\int_{-\infty}^{\infty} i\omega H_j(-i\omega) G_{\dot{u}_k\ddot{u}_l}(i\omega)\, d\omega \tag{57}$$

$$\rho_{\dot{s}_{ki}\dot{s}_{lj}} = \frac{1}{\sigma_{\dot{s}_{ki}}\sigma_{\dot{s}_{lj}}}\int_{-\infty}^{\infty} (-\omega^2) H_i(i\omega) H_j(-i\omega) G_{\ddot{u}_k\ddot{u}_l}(i\omega)\, d\omega \tag{58}$$

Let $D_k(\omega_i, \xi_i)$ denote the response spectrum for the support degree of freedom k, representing the expected value of the peak of the velocity response of an oscillator of frequency ω_i and damping ξ_i to the base acceleration $\ddot{u}_k(t)$. Likewise, $\dot{u}_{k,max}$ denotes the mean peak ground velocity. Eventually, the maximum strain rate under multiple-support excitations, i.e., $|\dot{\varepsilon}(t)|'_{max}$, can be calculated by the following equation

$$|\dot{\varepsilon}(t)|'_{max} = [\sum_{k=1}^{m}\sum_{l=1}^{m} \boldsymbol{a}_k \boldsymbol{a}_l \rho_{\dot{u}_k\dot{u}_l} \dot{u}_{k,max} \dot{u}_{l,max} + 2\sum_{k=1}^{m}\sum_{l=1}^{m}\sum_{j=1}^{N} \boldsymbol{a}_k \boldsymbol{b}_{lj} \rho_{\dot{u}_k\dot{s}_{lj}} \dot{u}_{k,max} D_l(\omega_j, \xi_j) + \sum_{k=1}^{m}\sum_{l=1}^{m}\sum_{i=1}^{N}\sum_{j=1}^{N} \boldsymbol{b}_{ki} \boldsymbol{b}_{lj} \rho_{\dot{s}_{ki}\dot{s}_{lj}} D_k(\omega_i, \xi_i) D_l(\omega_j, \xi_j)]^{1/2} \tag{59}$$

in which

$$\dot{u}_{k,max} = E[max|\dot{u}_k(t)|] \tag{60}$$

$$\dot{u}_{l,max} = E[max|\dot{u}_l(t)|] \tag{61}$$

$$D_k(\omega_i, \xi_i) = E[max|\dot{s}_{ki}(t)|] \tag{62}$$

$$D_l(\omega_j, \xi_j) = E[max|\dot{s}_{lj}(t)|] \tag{63}$$

5. Numerical examples

In order to investigate the effects of strain rate and ductility on the structural dynamic behavior and yield strength, the following exemplary structures are taken as examples to calculate their seismic responses.

The constitutive model for dynamic loading of steel material considering the strain rate effect (Li and Li 2010) is given by Eqs. (64)-(65)

$$f_{yd}/f_{ys} = 1 + c_y \lg(\dot{\varepsilon}_s/\dot{\varepsilon}_{s0}) \tag{64}$$

$$c_y = 0.1709 - 3.289 \times 10^{-4} f_{ys} \tag{65}$$

where $\dot{\varepsilon}_s$ and $\dot{\varepsilon}_{s0}$ denote the current strain rate and quasi-static strain rate, respectively; f_{yd} and f_{ys} denote the concrete compressive strength under dynamic and static loads. In general, $\dot{\varepsilon}_{s0}$ is equal to 2.5×10^{-4} s^{-1}.

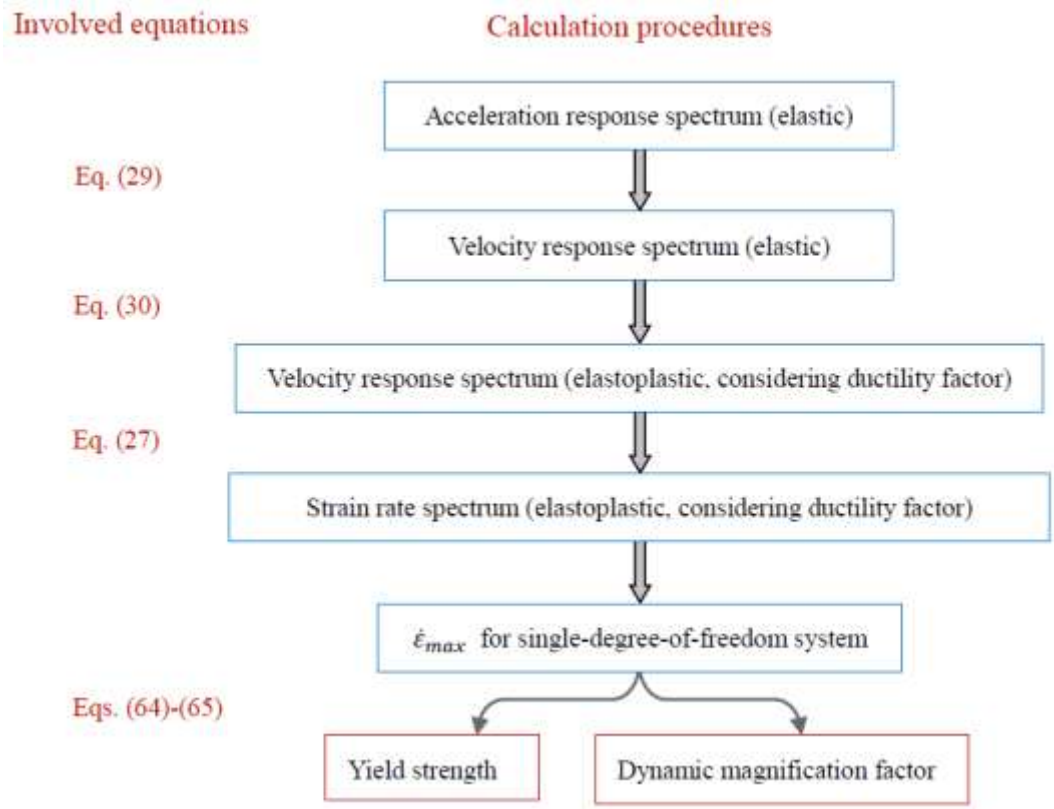

(a) SDOF system under uniform excitation

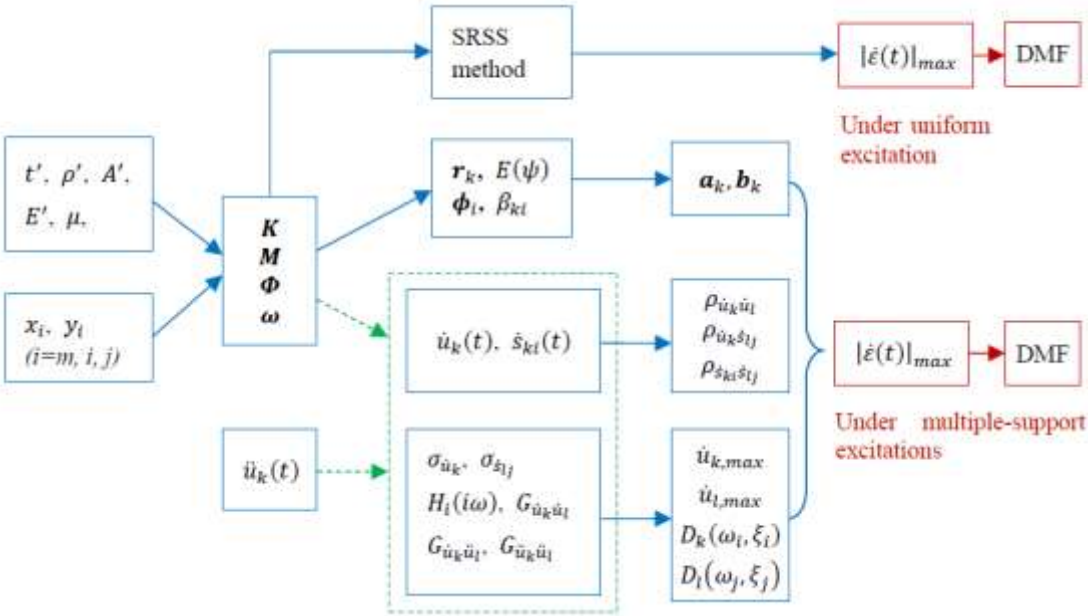

(b) MDOF systems under uniform and multiple-support excitations

Fig. 8 DMF calculation flowcharts considering the ductility and strain rate effects

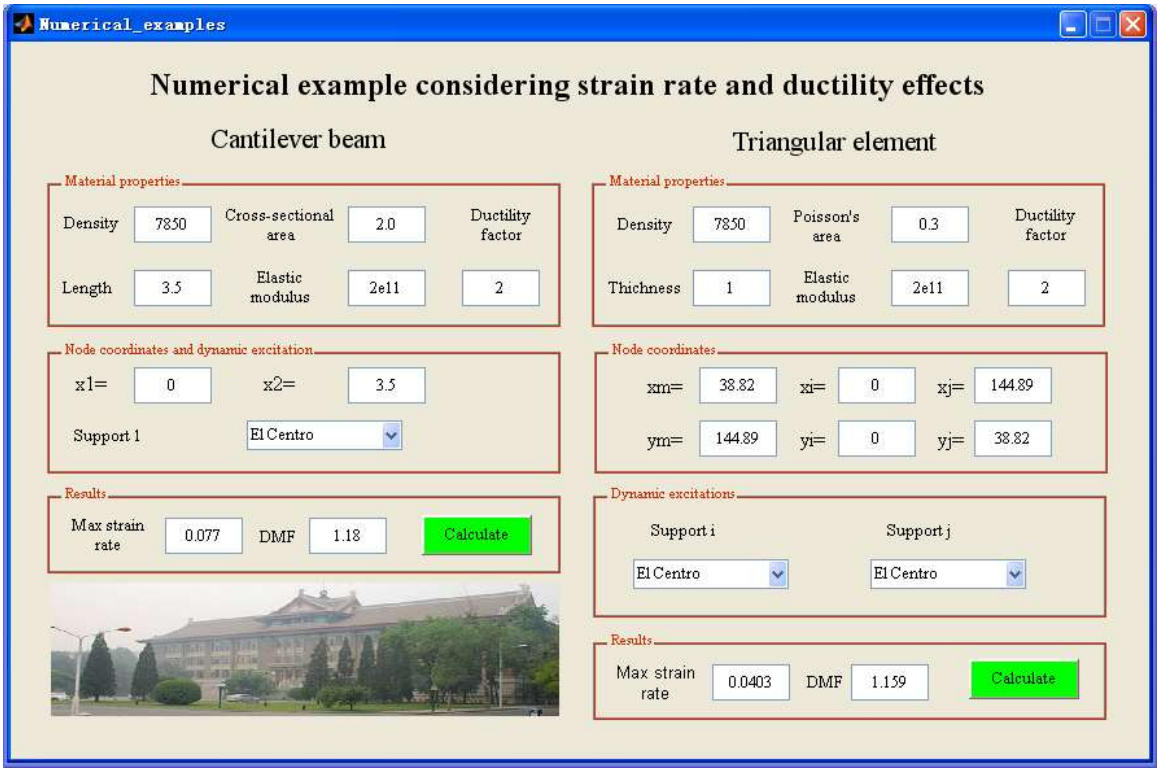

Fig. 9 Visual interface of the program

The DMF calculation flowcharts for SDOF and MDOF systems considering ductility and strain rate effects are illustrated in Fig. 8. It is convenient to estimate the maximum strain rate for SDOF system through the strain rate spectrum (see Fig. 7). For the MDOF system under uniform excitation, the total response can be obtained by superposing the response of each mode (Clough 1962, Singh and Mehta 1983, Sinha and Igusa 1995), and the SRSS modal combination method is adopted in this paper. Considering the spatially varying ground motions, a new response spectrum method developed in Section 4 can be employed for the calculation of the maximum strain rate. Therefore, three different numerical examples representing the above three cases respectively are given as follows. Moreover, a visual program shown in Fig. 9 is developed to perform the numerical calculation effectively and conveniently.

5.1 SDOF system under uniform excitation

The cantilever beam shown in Fig. 10 is taken as an example to investigate the effects of strain rate and ductility on the dynamic behavior and yield strength. In addition, the nodal coordinates in Fig. 10 remain the same as those in Fig. 6(a). Therefore, the strain rate spectrum illustrated in Fig. 7(a) is still available.

As shown in Fig. 10, the axial motion and deformation of the cantilever beam are merely considered in the analysis. Furthermore, the total mass and stiffness matrices, $\boldsymbol{M}_{total}$ and $\boldsymbol{K}_{total}$, are expressed as

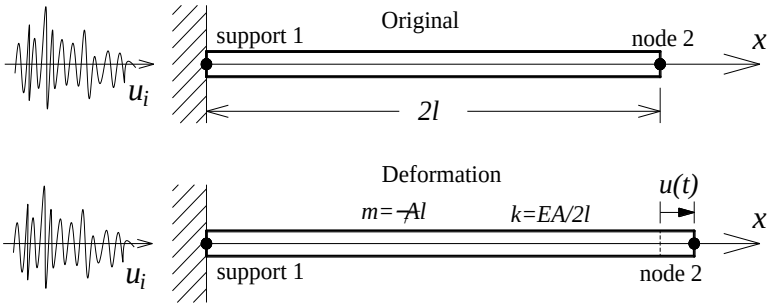

**m* and *k* denote the lumped mass and stiffness, respectively; *E* and *ρ* denote the modulus of elasticity and density, respectively; *A* and *l* denote the cross-sectional area and length of the cantilever beam.

Fig. 10 Cantilever beam (one-dimensional)

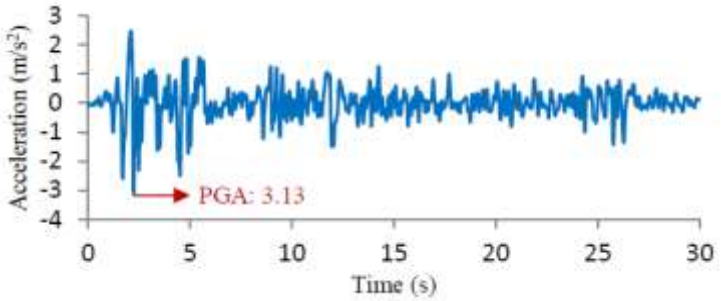

Fig. 11 El Centro earthquake acceleration history

$$\boldsymbol{M}_{total} = \rho Al \begin{bmatrix} 1 & 0 \\ 0 & 1 \end{bmatrix} \tag{66}$$

$$\boldsymbol{K}_{total} = \frac{EA}{2l} \begin{bmatrix} 1 & -1 \\ -1 & 1 \end{bmatrix} \tag{67}$$

where $\rho Al = 5.8 \times 10^7$Kg and $EA/2l = 6.0 \times 10^{10}$N/m.

The El Centro earthquake ground motion shown in Fig. 11 is selected as the dynamic excitation and the peak ground acceleration (PGA) is highlighted.

According to Eq. (40), the dynamic response can be calculated by Newmark-β explicit method (Clough and Penzien 1993, Chopra 2001). The integration step is 0.0002 s and the parameters γ and β are equal to 0.5 and 0.25, respectively. The displacement response of the corresponding elastic system is given in Fig. 12 and the internal force *f* shown in Fig. 13 is obtained directly by the following equation

$$f = ku_2 \tag{68}$$

where *k* denotes the axial stiffness of the cantilever beam; u_2 denotes the deformation of node *2*.

In Fig. 13, the original yield strength without considering the ductility and strain rate effects is equal to 300 MPa, and plastic deformation occurs at certain moments. Considering the ductility and strain rate effects, the dynamic yield strength increases and the yield deformation may be

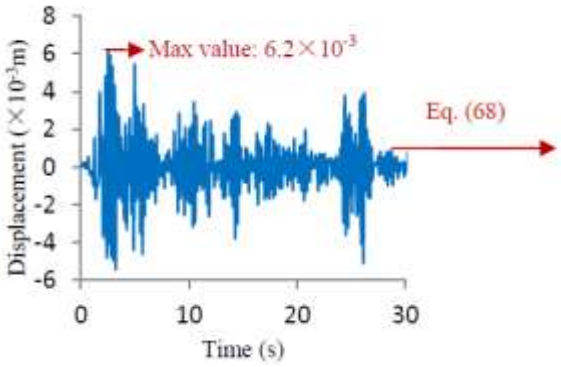

Fig. 12 Displacement response of the corresponding elastic system

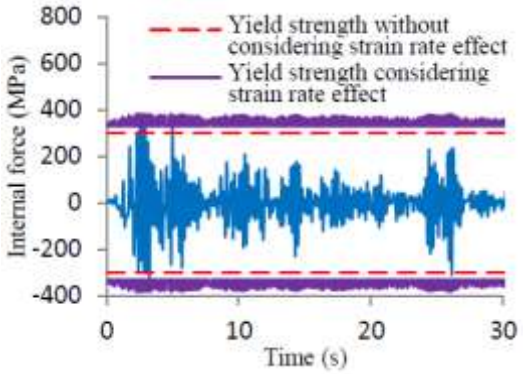

Fig. 13 Yield conditions in the cases of with and without considering strain rate effect

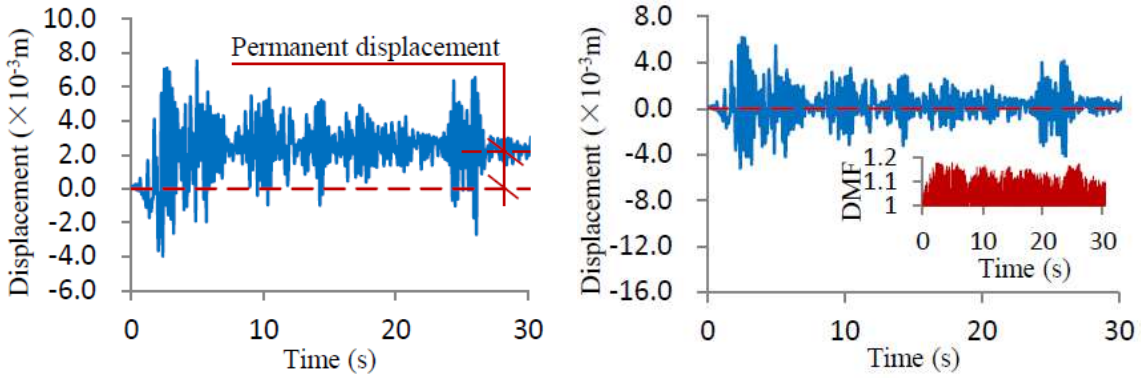

(a) Considering only the ductility effect (b) Considering both ductility and strain rate effects

Fig. 14 Displacement responses of cantilever beam

significantly different. The displacement response and DMF history in time domain are given in Fig. 14. The results show that the permanent deformation without considering the strain rate effect reaches 2.3×10^{-3} m. However, the permanent deformation is close to 0 if the ductility and strain rate effects are taken into consideration. It is necessary to consider the effects of ductility and strain rate on structural dynamic response in practical engineering accordingly.

In practice, it is known that the strength demand is reduced with increasing ductility factor and strain rate, and even small amount of inelastic deformation produces a significant reduction in the strength demand (Chopra 2001). Current seismic design methods are based on an estimate of the elastic strength demand that is decreased based on a "response modification factor" (UBC 1997, IBC 2003), which is implicitly related to the system overstrength and displacement ductility capacity (Medina and Krawinkler 2005), to estimate the design strength demand. Considering the reduction effects produced by the ductility and strain rate, the strength demand can be quantitatively estimated based on Eqs. (30), (64)-(65).

As shown in Table 1, four cases are discussed. In Case 1, the effects of ductility and strain rate on the strength demand are ignored in the analysis; in Case 2, only the ductility effect is considered; in Case 3, only the strain rate effect is considered; and in Case 4, both the ductility and

Table 1 Strength demand in different cases

Case	Strength demand f_y (MPa)			
	Elastic system	Elastoplastic system		
	μ=1	μ=1.5	μ=2	μ=4
1	300	300	300	300
2	300	212.1	173.2	113.4
3	250.6	250.6	250.6	250.6
4	250.6	179.0	146.8	97.3

strain rate effects are considered. Results show that in combination of ductility and strain rate effects, the strength demand decreases significantly.

5.2 MDOF system under uniform excitation

As illustrated in Fig. 15, the triangular element is given for investigating the effects of strain rate and ductility on the structual dynamic behavior and yield strength. The calculation procedures are shown in Fig. 8 and the aforementioned program is adopted. Moreover, the total mass and stiffness matrices, $\boldsymbol{M}'_{total}$ and $\boldsymbol{K}'_{total}$, are given as follows

$$\boldsymbol{M}'_{total} = \left[\begin{array}{c|cc} \boldsymbol{M}' & \boldsymbol{M}'_c \\ \hline (\boldsymbol{M}'_c)^T & \boldsymbol{M}'_g \end{array}\right] = \left[\begin{array}{c|cc} \boldsymbol{m}'_{mm} & \boldsymbol{m}'_{mi} & \boldsymbol{m}'_{mj} \\ \hline \boldsymbol{m}'_{im} & \boldsymbol{m}'_{ii} & \boldsymbol{m}'_{ij} \\ \boldsymbol{m}'_{jm} & \boldsymbol{m}'_{ji} & \boldsymbol{m}'_{jj} \end{array}\right] \tag{69}$$

$$\boldsymbol{K}'_{total} = \left[\begin{array}{c|cc} \boldsymbol{K}' & \boldsymbol{K}'_c \\ \hline (\boldsymbol{K}'_c)^T & \boldsymbol{K}'_g \end{array}\right] = \left[\begin{array}{c|cc} \boldsymbol{k}'_{mm} & \boldsymbol{k}'_{mi} & \boldsymbol{k}'_{mj} \\ \hline \boldsymbol{k}'_{im} & \boldsymbol{k}'_{ii} & \boldsymbol{k}'_{ij} \\ \boldsymbol{k}'_{jm} & \boldsymbol{k}'_{ji} & \boldsymbol{k}'_{jj} \end{array}\right] \tag{70}$$

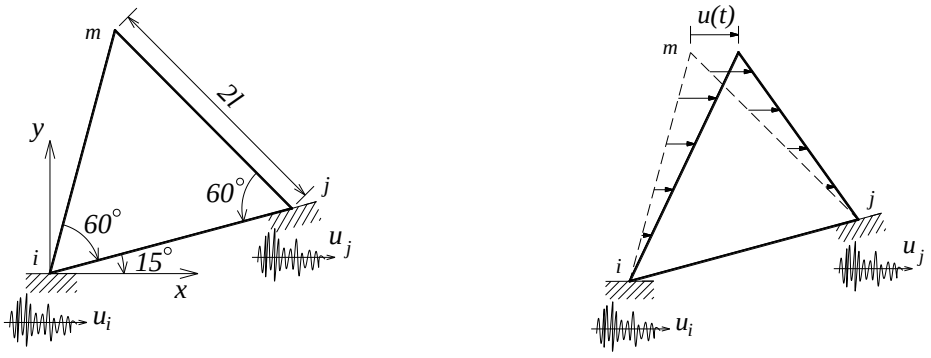

(a) Original triangular element (b) Deformed triangular element

*Supports *i* and *j* are completely fixed; node *m* has two degrees of freedom in *x* and *y* direction, respectively.

Fig. 15 Triangular element under uniform excitation

where $\boldsymbol{M}'$ and $\boldsymbol{K}'$ are the mass and stiffness matrices associated with the unconstrained degrees of freedom, respectively; $\boldsymbol{M}_g'$ and $\boldsymbol{K}_g'$ are the mass and stiffness matrices associated with the support degrees of freedom, respectively; $\boldsymbol{M}_c'$ and $\boldsymbol{K}_c'$ are coupling mass and stiffness matrices associated with both unconstrained and support degrees of freedom; the subscripts *m*, *i* and *j* relate to the associated variable of node *m*, *i* and *j*.

Only the submatrices $\boldsymbol{M}'$, $\boldsymbol{M}_c'$, $\boldsymbol{K}'$ and $\boldsymbol{K}_c'$ in Eq. (40) are involved in the calculation. Herein, $\boldsymbol{M}_c'$ is a null matrix due to the lumped mass matrix adopted in this numerical example; $\boldsymbol{M}'$ and $\boldsymbol{K}'$ can be calculated by following equations

$$\boldsymbol{M}' = \boldsymbol{m}_{mm}' = \frac{\rho' A' t'}{3}\begin{bmatrix}1 & 0\\ 0 & 1\end{bmatrix} \tag{71}$$

$$\boldsymbol{K}' = \boldsymbol{k}_{mm}' = \frac{E' t'}{4\left(1-\mu'^2\right)A'}\begin{bmatrix} b_m^2 + \frac{1-\mu'}{2}c_m^2 & \frac{1+\mu'}{2}b_m c_m \\ \frac{1+\mu'}{2}c_m b_m & c_m^2 + \frac{1-\mu'}{2}b_m^2 \end{bmatrix} \tag{72}$$

$$b_m = -\begin{vmatrix}1 & y_i\\ 1 & y_j\end{vmatrix} \tag{73}$$

$$c_m = \begin{vmatrix}1 & x_i\\ 1 & x_j\end{vmatrix} \tag{74}$$

where E', μ' and ρ' denote elasticity modulus, Poisson's rate and density, respectively; A' and t' denote the cross-sectional area and thickness of the triangular element; $\rho' A' t'/3$ is set to 2.832×10^4 kg; $E' t'/4(1-\mu^2)A'$ is set to 50.758 N/m^3.

The coupled stiffness matrix $\boldsymbol{K}_c'$ can be obtained based on the condition of static equilibrium due to the supports *i* and *j* are completely fixed

$$\boldsymbol{K}_c' = \begin{bmatrix}\boldsymbol{k}_{mi}' & \boldsymbol{k}_{mj}'\end{bmatrix} = \begin{bmatrix} 2.7322k_a & -0.7321k_b & -3.7322k_a & -0.2679k_b \\ 2.7322k_b & -0.7321k_c & -3.7322k_b & -0.2679k_c \end{bmatrix} \tag{75}$$

$$k_a = \frac{E' t'}{4(1-\mu^2)A}\left(b_m^2 + \frac{1-\mu}{2}c_m^2\right) \tag{76}$$

$$k_b = \frac{E' t'}{4(1-\mu^2)A}\frac{1+\mu}{2}b_m c_m \tag{77}$$

$$k_c = \frac{E' t'}{4(1-\mu^2)A}\left(c_m^2 + \frac{1-\mu}{2}b_m^2\right) \tag{78}$$

The El Centro earthquake acceleration history shown in Fig. 11 is selected as the uniform dynamic excitation for the triangular element. To analyze how the elastoplastic displacement response of triangular element is affected by the strain rate effect, the dynamic excitation is magnified 20 times to make the structure yield. The stress history at node *m* can be calculated by following equations

$$\begin{bmatrix}\sigma_x\\ \sigma_y\\ \tau_{xy}\end{bmatrix} = \frac{E}{1-\mu^2}\begin{bmatrix}1 & \mu & \\ \mu & 1 & \\ & & \frac{1-\mu}{2}\end{bmatrix}\begin{bmatrix}\varepsilon_x\\ \varepsilon_y\\ \gamma_{xy}\end{bmatrix} \tag{79}$$

$$\varepsilon_x = \left|\frac{\partial(\psi_t)}{\partial x}\right| u_x \tag{80}$$

$$\varepsilon_y = \left|\frac{\partial(\psi_t)}{\partial y}\right| u_y \tag{81}$$

where σ and τ denote the normal and shear stress, respectively; ε and γ denote the normal and shear strain, respectively. For the steel material, elastic modulus and Poisson's rate are equal to 2×10^{11} Pa and 0.3, respectively.

The horizontal displacement and stress responses are given in Figs. 16-17, and the maximum value of displacement response is highlighted. In Fig. 17, the original yield strength without considering the strain rate effects is equal to 300 MPa. The dynamic yield strength increases under the effect of ductility and strain rate, thus the displacement response will be different. In general, the permanent displacement tends to decrease with increasing yield strength, but this trend is not absolute because the permanent displacement depends not only on the yield strength but also on the characteristics of the ground motion.

As shown in Fig. 18, the displacement response and DMF history in time domain under uniform excitation is given. For the displacement response without considering the strain rate

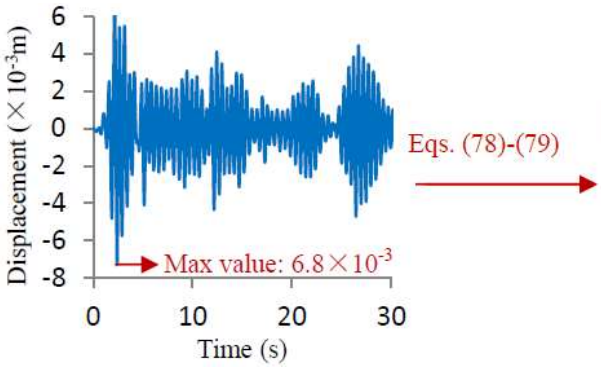

Fig. 16 Displacement response of the corresponding elastic system

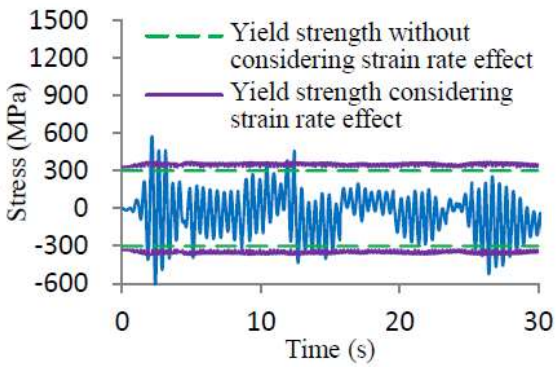

Fig. 17 Yield conditions in the cases of with and without considering strain rate effect

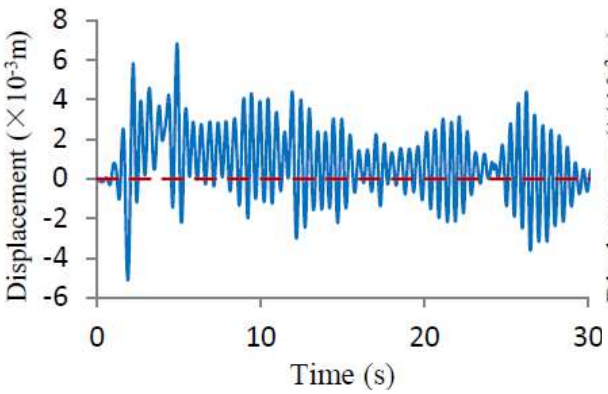

(a) Considering only the ductility effect

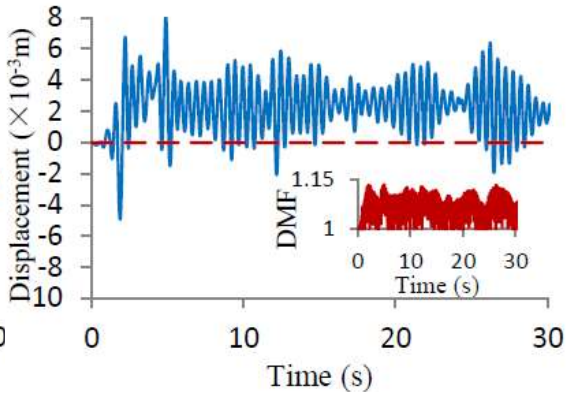

(b) Considering both ductility and strain rate effects

Fig. 18 Displacement responses of triangular element under uniform excitation

Table 2 Strength demand in different cases

Case	Strength demand f_y (MPa)			
	Elastic system	Elastoplastic system		
	μ=1	μ=1.5	μ=2	μ=4
1	300	300	300	300
2	300	256.1	236.6	206.7
3	254.7	254.7	254.7	254.7
4	254.7	220.0	204.1	180.7

effect, the permanent deformation at the end of seismic excitation is close to 0 because the yield deformations in the positive and negative directions cancel each other out. For the displacement response considering the ductility and strain rate effects, the permanent deformation is approximately 1.7×10^{-3} m. The reason is that due to the increase in yield strength, yield deformation in the negative direction is reduced more significantly than that in the positive direction.

Considering the reduction effects produced by the ductility and strain rate, the strength demand can be quantitatively estimated using Eqs. (30), (64)-(65). Four cases included in Table 2 are identical to those in Table 1.

In Table 2, results show that with the consideration of ductility and strain rate effects, the strength demand of the system to limit the ductility demand imposed by the ground motion to a specified value decreases significantly.

5.3 MDOF system under multiple-support excitations

The numerical example shown in Fig. 19 is almost the same as that shown in Fig. 15, and the only difference is that the multiple-support (instead of uniform) excitations is adopted. In addition, El Centro and Kobe earthquake acceleration histories recorded at firm-soil condition are selected as the dynamic excitation at support *i* and *j*, respectively. As shown in Fig. 20, the Kobe earthquake acceleration history is given and the PGA is highlighted. In order to analyze how the elastoplastic displacement response of triangular element is affected by the strain rate effect, the El Centro and Kobe acceleration histories are magnified 10 and 3.82 times (the PGAs of two acceleration histories are equal) to make the structure yield.

For a simple MDOF system like the numerical example given herein, the dynamic response of the triangular element in time domain can be calculated based on Eq. (40) by numerical time-stepping algorithm. The horizontal displacement and stress responses are given in Figs. 21-22, respectively, and the maximum value of displacement response is highlighted. As illustrated in Fig. 22, the original yield strength without considering the strain rate effects is equal to 300 MPa, and the plastic deformation occurs at certain moments. In combination of the ductility and strain rate effects, the dynamic yield strength increases and the permanent displacement may be significantly different.

The displacement response and DMF history in time domain under multiple-support excitations are given in Fig. 23. Due to the amplification effect of the strain rate on the yield strength, the yield deformation in the negative direction shown in Fig. 23(a) is larger than that shown in Fig. 23(b). For the displacement response without considering the strain rate effect, the permanent

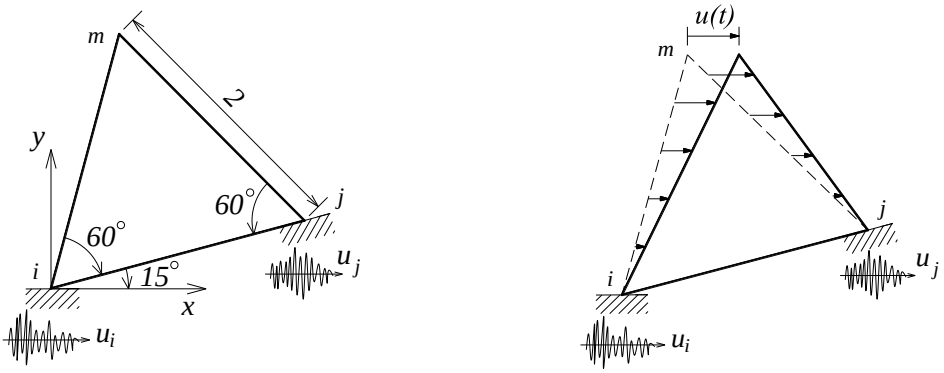

(a) Original triangular element (b) Deformed triangular element

*Supports *i* and *j* are completely fixed; node *m* has two degrees of freedom in *x* and *y* direction, respectively

Fig. 19 Triangular element under multiple-support excitations

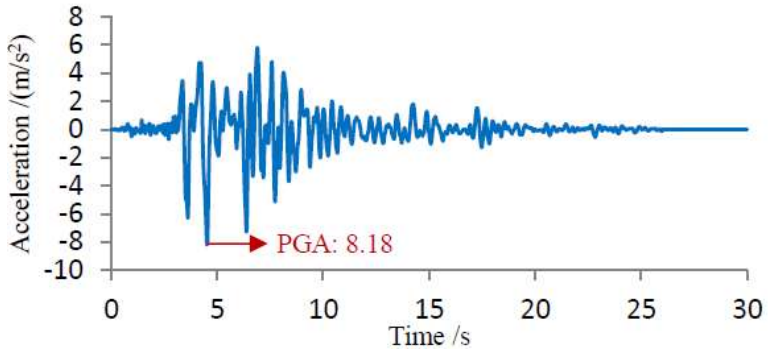

Fig. 20 Kobe earthquake acceleration history

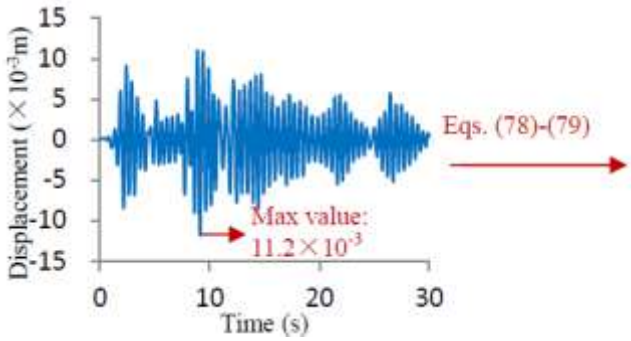

Fig. 21 Displacement response of the corresponding elastic system

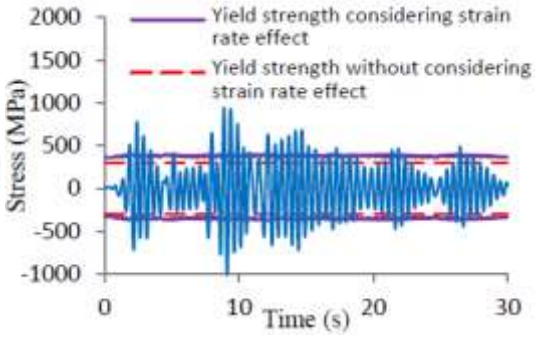

Fig. 22 Yield conditions in the cases of with and without considering strain rate effect

deformation at the end of seismic excitation is equal to -8.9×10^{-3}m. However, for the displacement response considering the ductility and strain rate effects, the permanent deformation is approximately 2.3×10^{-3} m. The results indicate that the difference between deformations with and without considering strain rate effect is significant and unnegligible.

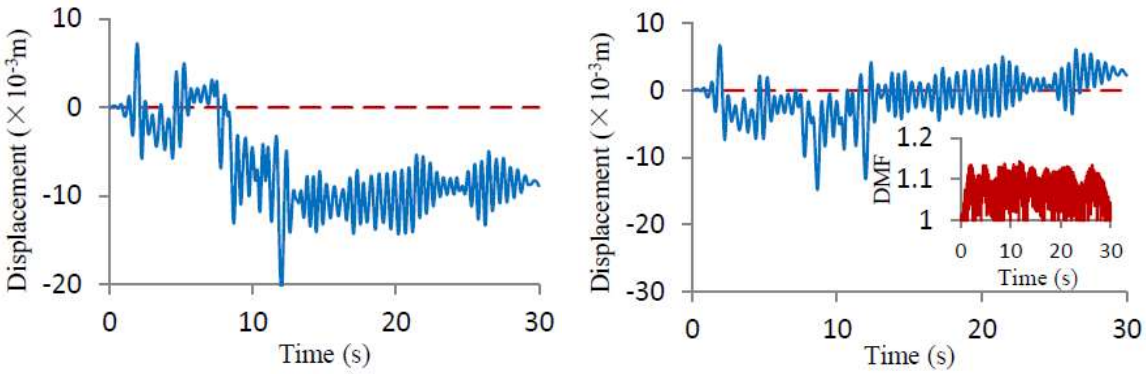

(a) Considering only the ductility effect (b) Considering both ductility and strain rate effects

Fig.23 Displacement responses of triangular element under multiple-support excitatio

Table 3 Strength demand in different cases

Case	Strength demand f_y (MPa)			
	Elastic system	Elastoplastic system		
	μ=1	μ=1.5	μ=2	μ=4
1	300	300	300	300
2	300	256.1	236.6	206.7
3	250.0	250.0	250.0	250.0
4	250.0	213.4	199.7	178.2

Based on the response spectrum method developed in Section 4, the maximum strain rate of triangular element under multiple-support excitation can be calculated. Considering the reduction effects produced by the ductility and strain rate, the strength demand can be quantitatively estimated based on Eqs. (30), (64)-(65). Four cases included in Table 3 are the same as those in Tables 1-2.

The strength demand decreases significantly under the effects of strain rate and ductility. In addition, as shown in Fig. 7 in section 3, the increasing ductility factor has a reduction effect on strain rate, which makes the yield strength decrease indirectly.

6. Conclusions

The effects of ductility and strain rate on the structural dynamic behaviors and yield strength are investigated in this paper. On the basis of theoretical deduction, three numerical models are taken as examples to calculate their displacement response and strength demand. The main conclusions are summarized as follows.

• The relationship between relative velocity and strain rate response is deduced and the strain rate spectrum is presented. The ductility factor is incorporated into the strain rate spectrum based on the constant-ductility velocity response spectrum. It is convenient to estimate the maximum strain rate of the structure through the strain rate spectrum.

• Considering the spatially varying ground motions, a new response spectrum method is developed by incorporating the ductility factor and the strain rate into the conventional response spectrum method to estimate the maximum strain rate of structure.

• Numerical results show that the permanent displacements, as well as the deformation histories, are significantly influenced by strain rate effect. Furthermore, considering the ductility and strain rate effects, the strength demands are significantly reduced. The results indicate that it is not only necessary in theory but also significant in engineering practice to take the ductility and strain rate effects into consideration.

Acknowledgments

This work was supported by the National Natural Science Foundation of China (Grant Nos. 51408409, 51579173 and 51379140) and the Tianjin Research Program of Application Foundation and Advanced Technology (Grant No. 15JCQNJC07400).

References

Alzubaidi, R. and Lafta, S.H. (2013), "Effect of strain rate on the strength characteristics of soil-lime mixture", *Geotech. Geol. Eng*., **31**(4), 1317-1327.

Carlson, C.P., Zekkos, D. and Mccormick, J.P. (2014), "Impact of time and frequency Domain ground motion modification on the Response of a SDOF system", *Earthq. Struct*., **7**(6), 1283-1301.

Cervera, M., Oliver, J. and Manzoli, O. (1996), "A rate-dependent isotropic damage model for theseismic analysis of concrete dams", *Earthq. Eng. Struct. Dyn*., **25**(9), 987-1010.

Chopra, A.K. (2001), *Dynamics of Structures: Theory and Applications to Earthquake Engineering, 2nd*, Prentice Hall, Englewood Cliffs, New Jersey, USA.

Chopra, A.K. and Chintanapakdee, C. (2004), "Inelastic deformation rates for design and evaluation of structures: single-degree-of-freedom bilinear systems", *J. Struct. Eng*., **130**(9), 1310-1319.

Clough, R.W. (1962), "Earthquake analysis by response spectrum superposition", *Bull. Seismol. Soc. Amer.*, **52**(3), 693-697.

Clough, R.W. and Penzien, J. (1993), *Dynamics of Structures. 2nd*, McGraw-Hill, USA.

COMITE EURO-INTERNATIONAL DU BETON. (1990), *CEBFIP model code 1990*, Redwood Books, Trowbridge, Wiltshire, Great Britain.

Guo, W., Yu, Z.W., Liu, G.H. and Guo, Z. (2013), "Possible existing seismic analysis errors of long span structures and bridges while utilizing multi-point earthquake calculation models", *Bull. Earthq. Eng.*, **11**(5), 1683-1710.

Hao, H. (1991), "Response of multiply-supported rigid plate to spatially correlated seismic excitations", *Earthq. Eng. Struct. Dyn*., **20**(9), 821-838.

Hao, H. and Xiao, N.D. (1996), "Multiple excitation effects on response of symmetric buildings", *Eng. Struct.*, **18**(9), 732-740.

Huh, H., Lin, J.H. and Park, S.H. (2009), "High speed tensile test of steel sheets for the stress-strain curve at the intermediate strain rate", *Int. J. Auto. Technol.*, **10**(2), 195-204.

International Code Council (2003), *International Building Code (IBC)*, Falls Church, Virginia, USA.

International Conference of building Officials (1997), *Uniform Building Code (UBC)*, Whittier, California, USA.

Kiureghian, A.D. and Neumnhofer, A. (1992), "Response spectrum method for multiple-support seismic excitations", *Earthq. Eng. Struct. Dyn.*, **21**(8), 713-740.

Li, G. and Larry, A. Fahnestock (2013), "Seismic response of single-degree-of-freedom systems representing

low-ductility steel concentrically-braced frames with reserve capacity", *J. Struct. Eng.*, **139**(2), 199-211.
Li, M. and Li, H.N. (2010), "Dynamic test and constitutive model for reinforcing steel", *China Civ. Eng. J.*, **43**(4), 70-75. (in Chinese)
Li, M. and Li, H.N. (2012), "Effects of strain rate on reinforced concrete structure under seismic loading", *Adv. Struct. Eng.*, **15**(3), 461.
Medina, R.A. and Krawinkler, H. (2005), "Strength demand issues relevant for the seismic design of moment-resisting frames", *Earthq. Spectra*, **21**(2), 415-439.
Shing, P.S.B. and Mahin, S.A. (1988), "Rate-of-Loading Effects on Pseudodynamic Tests", *J. Struct. Eng.*, **114**(11), 2403-2420.
Singh, M.P. and Mehta, K.B. (1983), "Seismic design response by an alternative SRSS rule", *Earthq. Eng. Struct. Dyn.*, **11**(6), 771-783.
Sinha, R. and Igusa, T. (1995), "CQC and SRSS methods for non-classically damped structures", *Earthq. Eng. Struct. Dyn.*, **24**(4), 615-619.
Su, L. and Shi, J.T. (2013), "Displacement-based earthquake loss assessment methodology for RC frames infilled with masonry panels", *Eng. Struct.*, **48**, 430-441.
Su, L., Dong, S.L. and Kato, S. (2006), "A new average response spectrum method for linear response analysis of structures to spatial earthquake ground motions", *Eng. Struct.*, **28**(13), 1835-1842.
Tian, L. and Li, H.N. (2010), "Seismic response of power transmission tower-line system subjected to spatially varying ground motions", *Math. Prob. Eng.*, **2010**, 587317.
Tian, L., Ma, R.S., Li, H.N. and Zhang, P. (2014), "Seismic response of straight line type and broken line type transmission lines subjected to non-uniform seismic excitations", *Adv. Steel Constr.*, **10**(1), 85-98.
Wang, W.M., Li, H.N. and Tian, L. (2013), "Progressive collapse analysis of transmission tower-line system under earthquake", *Adv. Steel Constr.*, **9**(2), 161-172.
Xu, Z.D. (2010), "Review for dynamic researches in civil engineering in recent years", *Sci, China Technol. Sci.*, **53**(5), 1450-1452.
Yu, R.F. and Zhou, X.Y. (2008), "Response spectrum analysis for non-classically damped linear system with multiple-support excitations", *Bull. Earthq. Eng.*, **6**(2), 261-284.
Zhai, C.H. and Xie, L.L. (2007), "Progress on strength reduction factors in structural seismic design", *J. Harbin Inst. Tech.*, **39**(8), 1177-1184. (in Chinese)

CC